https://doi.org/10.5194/os-2021-107
Preprint. Discussion started: 8 November 2021

Ocean Science
Discussions
Open Access
EGU

Technical note: Turbulence measurements from a Light Autonomous Underwater Vehicle

Eivind H. Kolås[1], Tore Mo-Bjørkelund[2], and Ilker Fer[1]

[1]Geophysical Institute, University of Bergen and Bjerknes Center for Climate Research, Bergen, Norway
[2]Norwegian University of Science and Technology, Trondheim, Norway

Correspondence: Eivind H. Kolås (eivind.kolas@uib.no)

Abstract. A self-contained turbulence instrument from Rockland Scientific was installed on a Light Autonomous Underwater Vehicle (AUV) from OceanScan Marine Systems and Technology Lda. We report on the data quality and discuss limitations of dissipation estimated from two shear probes during a deployment in the Barents Sea in February 2021. The AUV mission lasted for 5 hours, operating at a typical horizontal speed of $1.2\,\mathrm{m\,s^{-1}}$. The AUV was programmed to find and cross the maximum along-path thermal gradient at 10, 20 and 30 m depths along $4\,\mathrm{km}$ transects. Although the AUV vibrations contaminate the shear probe records, the noise is mitigated by removing vibration-induced components from shear spectra using accelerometer signal measured in multiple directions. Dissipation rate estimates in the observed transects varied in the range 1×10^{-8} and $6 \times 10^{-6}\,\mathrm{W\,kg^{-1}}$, with the values from the two orthogonal probes typically in agreement to within a factor of 2. Dissipation estimates from the AUV show good agreement with nearby vertical microstructure profiles obtained from the ship during the transects, indicating that the turbulence measurements from the AUV are reliable for this relatively turbulent environment. However, the lowest reliable dissipation rates are limited to $5 \times 10^{-8}\,\mathrm{W\,kg^{-1}}$, making this setup unfit for use in quiescent environments.

1 Introduction

Turbulence measurements in the ocean are needed to quantify the turbulent fluxes of heat, salt and momentum, and are important for understanding the processes affecting evolution and transformation of water masses, their heat and salt content, and distribution of nutrients. The dissipation rate of turbulent kinetic energy provides the energy that homogenizes the gradients of temperature and salinity. Quantifying the magnitude and distribution of the dissipation rate helps identify the different forcing mechanisms and their relative contribution in mixing. In general, the necessary requirements for measuring ocean turbulence can be summed up in three elements: a sensor or probe that detects the physical parameter of interest; an electronic circuitry that amplifies and filters the signal produced by the probe; and a stable platform that is rigid or moves smoothly in the ocean (Lueck et al., 2002).

https://doi.org/10.5194/os-2021-107
Preprint. Discussion started: 8 November 2021

Holding a probe stable while moving it smoothly through a dynamic ocean is not trivial. Ocean waves, currents and controlled platform adjustments will lead to platform motion and artificial signals not associated with natural turbulence. The most common method for measuring ocean turbulence is to measure the small-scale velocity shear by using free-falling or loosely-tethered vertical microstructure profilers equipped with airfoil shear probes (Lueck, 2005; Gregg, 2021). Such profilers are commonly deployed from moving vessels or drifting sea ice. However, the traditional methods limit the spatial and temporal coverage of the measurements. Robotic platforms offer the potential to greatly increase the availability of ocean-mixing measurements (Frajka-Williams et al., 2022).

Robotic platforms such as Autonomous Underwater Vehicles (AUVs) and ocean gliders enable turbulence measurements in a variety of patterns and detect structures that may be left undetected using vertical profiling alone (Yamazaki et al., 1990; Frajka-Williams et al., 2022). However, obtaining high-quality turbulence measurements from robotic platforms can be challenging. The vehicle motion, both forward motion and maneuvering, must be resolved and its effect on the measured signal must be filtered out. Pioneering work in the 90s used turbulence measurement packages and three orthogonal accelerometers mounted on AUVs, such as described by Levine and Lueck (1999) and Dhanak and Holappa (1999). Vehicle vibrations were found to completely obscure oceanic signals at distinct frequencies. Using coherency analysis between the shear probe record and the acceleration measured by the accelerometer aligned with the shear probe, noise could be removed in the time and frequency domain (Levine and Lueck, 1999). Goodman et al. (2006) improved this technique and developed a multivariate correction approach to remove vibration-induced components from shear spectra using accelerometer signal measured in multiple directions. This latter way of minimizing the effects of body motion and probe vibrations on the turbulence measurements is commonly known as the "Goodman method", and paved the way for a range of robotic platforms with microstructure sensors.

Modern microstructure measurements using shear probes attached to robotic platforms include those from gliders (Fer et al., 2014; Palmer et al., 2015; Schultze et al., 2017; Scheifele et al., 2018), and from AUVs such as REMUS (Goodman et al., 2006) and the Autosub Long Range AUV (Thorpe et al., 2003; McPhail et al., 2019; Garabato et al., 2019; Spingys et al., 2021). Gliders are buoyancy driven and, in contrast to AUVs, do not use a thruster for forward motion (some new generation gliders, however, are equipped with a thruster for rapid maneuvering when needed). The smooth motion of the gliders with negligible vehicle vibration and signal contamination makes them excellent platforms for shear probe measurements (Fer et al., 2014). While offering extended endurance of 1 to 3 months, gliders move relatively slow (0.1–0.3 $\mathrm{m\,s^{-1}}$ through water) and typically profile in a saw-tooth pattern. AUVs move faster (order 1 $\mathrm{m\,s^{-1}}$ through water) and are more maneuverable, but have typically shorter endurance. A major concern regarding the quality of turbulence measurements from an AUV, is the vibrations caused by the thruster.

In this study, we mounted a self-contained turbulence instrument package on a Light AUV, and collected measurements in the Barents Sea in a frontal region where Atlantic- and Arctic-origin waters meet (Figure 1). The Light AUV is lighter and more affordable than REMUS and the Autosub Long Range AUV, and enables easy deployment and recovery. In this technical note we describe the instrument setup and the data collected (Sect. 2), the processing methods (Sect. 3), and present the data quality and the capability of the Light AUV for dissipation rate measurements (Sect. 4). In our notation, data processing and format

https://doi.org/10.5194/os-2021-107
Preprint. Discussion started: 8 November 2021

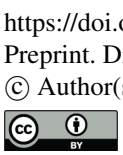

Ocean Science
Discussions
Open Access
EGU

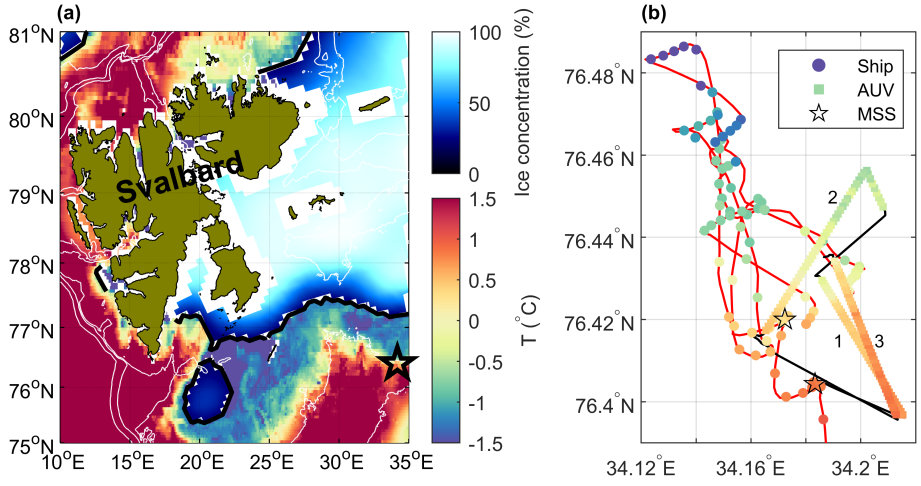

Figure 1. a) Overview map of the study region in the Barents Sea. White isobaths are drawn at 250, 500 and 1000 m depth using IBCAO-v3 (Jakobsson et al., 2012). Ice concentration and ice edge (thick black contour) on 26 February 2021 is from OSI SAF (OSI SAF, 2017). Sea surface temperature is from the product SEAICE_ARC_SEAICE_L4_NRT_OBSERVATIONS_011_008 at 0.05° resolution based upon observations from the Metop_A AVHRR instrument.Experiment location marked by a star near 34°E is expanded in (b). **b)** Ship's track (red) with near-surface temperature from the ship's thermosalinograph, and AUV's track (black) with AUV's temperature measurements along the three transects are color coded (temperature color scale is the same as in panel a). Stations where a vertical microstructure profile (MSS) was collected are also shown.

of the data, we follow the recommendations and conventions of the SCOR Working Group on analysing ocean turbulence observations to quantify mixing (ATOMIX) (http://wiki.uib.no/atomix). Data are made available from Fer et al. (2021).

2 Instruments, cruise and data

The data were collected during a Nansen Legacy cruise (9 February – 1 March 2021) on board the research icebreaker Kronprins Haakon, in the Barents Sea (Nilsen et al., 2021). Turbulence measurements using the Light AUV ("Harald", hereafter referred to as AUV) was made in the morning of 26 February 2021 near the Polar Front between Atlantic water and Polar water. The AUV was deployed at 07:30 UTC at 76°N 24.94' 34°E 9.61', and recovered at 12:15 UTC at 76°N 26.11' 34°E 11.21', after completing three crossings of the front. Before and during the AUV mission, the wind speed was around 10 m s^{-1} and air temperatures were close to -5°C, measured at 15 m height. The turbulence package on the AUV continuously measured ocean microstructure. Additional data used include near-surface temperature and salinity measured by a Sea-Bird Electronics thermosalinograph with water intake at 4 m depth, and two reference dissipation profiles measured by a vertical microstructure profiler (MSS-90L) from Sea and Sun Technology. The temperature and conductivity measured by the thermosalinograph are accurate to ± 0.001°C and ± 0.001 S m^{-1}. The noise level of the dissipation measurements from the MSS-90L is $(1-3) \times 10^{-9}$ W kg^{-1}. The ship track, AUV track and MSS positions are shown in Figure 1b.

https://doi.org/10.5194/os-2021-107
Preprint. Discussion started: 8 November 2021


Ocean Science Discussions

2.1 Light Autonomous Underwater Vehicle

The Light AUV was developed at the Underwater Systems and Technology Laboratory at the University of Porto (Sousa et al., 2012). It is commercially produced by OceanScan Marine Systems and Technology Lda. Our AUV is an extended version compared to the standard Light AUV. It is equipped with a pumped CTD (SBE-49 FastCAT, the instrument protruding from the nose of the AUV, Figure 2), a Nortek Doppler Velocity Log (DVL1000), an attitude sensor (Lord Microstrain 3DM-GX4-25), an acoustic modem, a Fluorescence sensor and a dissolved oxygen optode. The accuracy of the measurements from the AUV are ± 0.002°C for temperature, $\pm 0.0003\,\mathrm{S\,m^{-1}}$ for conductivity, 0.3% RMS (root mean square) of the measured value for horizontal flow speed past the instrument (measured by DVL1000), $\pm 8.5°$ for yaw at the observation latitude and $\pm 2.0°$ for pitch and roll. The AUV is controlled by the on-board software DUNE Unified Navigation Environment, and is configurable both in hardware and software. It is 100 m pressure rated. The turbulence package was mounted below the AUV using custom-made brackets, and connected to the AUV using a bulkhead connector and a custom-made cable.

Before deployment, the AUV was programmed to detect the maximum of the temperature gradient along a North-South transect across a surface temperature front, and to adjust its trajectory to contain this gradient maximum in the subsequent transects. This was done by differentiating a Natural Cubic Spline regression of the temperature along the transect and finding the location of the absolute maximum of the temperature gradient, $\boldsymbol{x}_m$, after each transect. The location of the maximum gradient was then used in conjunction with the previous estimates of the front location to estimate the new front location, $\boldsymbol{x}_f$, by low-pass filtering the estimates:

$$\boldsymbol{x}_{f_k} = \boldsymbol{x}_{f_{k-1}} \cdot \alpha + \boldsymbol{x}_m \cdot (1 - \alpha)\,. \tag{1}$$

The initial estimate of the front location $\boldsymbol{x}_{f_1}$ was set by using data from the ship's thermosalinograph. The procedure in Eq. (1) was set to repeat for all the predefined transect depths, where $\boldsymbol{x}_{f_k}$ denotes the estimated front position for dive number k. $\alpha \in [0, 1]$ denotes the low pass filtering coefficient and was set to 0.5.

2.2 MicroRider

Turbulence measurements were made using a MicroRider-1000LP (MR) from Rockland Scientific, Canada. The MR was modified to the Tidal Energy (TE) configuration, earlier used in high flow tidal energy channels. The TE configuration includes increasing the sample rate to 1024 Hz for fast channels (from the typical 512 Hz), and replacing the ASTP circuit board components with an anti-aliasing filter of 196 Hz (from the typical 98 Hz), and reducing the gain of the shear channel by a factor of 10, from about 1 second to 0.1 second. This modification allows reaching wavenumbers high enough to resolve the shear spectrum (reaching 164 cpm at $1.2\,\mathrm{m\,s^{-1}}$ and with 196 Hz anti-aliasing filter). Reduction in the gain is to compensate for the larger signals produced by faster sensor speed through the water (the shear sensor signal increases in proportion to speed-squared).

The MR was attached beneath the AUV as seen in Figure 2. It was powered by a stand alone 4S1P (14.8V) Lithium Ion battery integrated in the vehicle, and controlled by a relay connected to the main power board inside the AUV. This was done

https://doi.org/10.5194/os-2021-107
Preprint. Discussion started: 8 November 2021

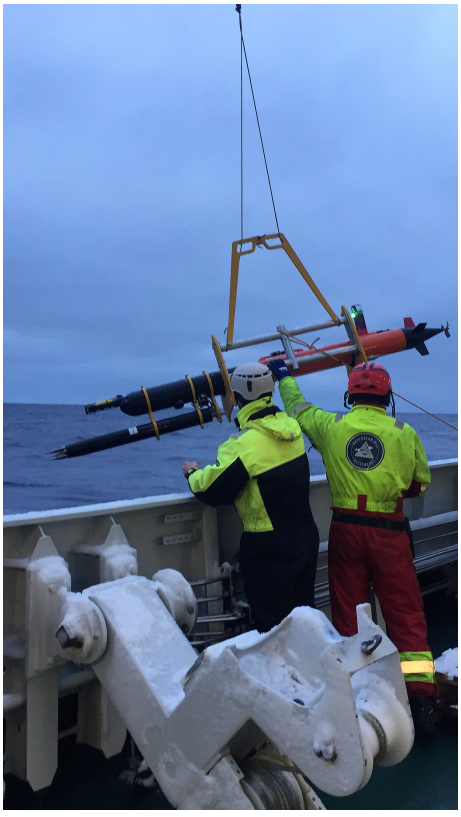

Figure 2. Deployment of MicroRider-1000LP mounted below the light AUV "Harald", in the Barents Sea, 07:30 on 26 February 2021. From left: Co-author Tore Mo-Bjørkelund and crew member Svein Are Simonsen. Photographer: Frank Nilsen, University Center at Svalbard

in order to provide a relatively clean power source. Earlier tests in a Norwegian fjord when the MR was fully integrated to the AUV power source, showed significant electronic noise in the microstructure measurements. Data were stored internally on a compact flash memory card. The vertical axis-to-axis separation between the AUV and the MR was approximately 30 cm. All turbulence sensors protruded about 25 cm from the nose of the AUV, outside the region of largest flow deformation.

The MR was equipped with two airfoil velocity shear probes (SPM-38), one fast-response thermistor (FP07), a pressure transducer, a two-axis vibration sensor (a pair of piezo-accelerometers), and a high-accuracy dual-axis inclinometer. The MR samples the signal plus signal derivatives on the thermistor and pressure transducer, and the derivative for shear signals, allowing high resolution measurements. The sampling rate is 1024 Hz for the vibration, shear and temperature sensors, and 128 Hz for pitch, roll and pressure. The accuracy of the measurements is 0.1% for the pressure, 2% for the piezo-accelerometers and 5% for the shear probes. Because of an error in the setup configuration file, the thermistor did not record measurements. Roll, pitch and yaw are clockwise rotations around the x, y and z axis of the AUV or the MR, following the right-hand rule. However, the instrument axis coordinate systems differ: for the MR x points outward from the nose along the instrument's axis, y is to the left (positive toward port) and z is positive upward. For the AUV, the vehicle xyz-frame is aligned with [North, East,

https://doi.org/10.5194/os-2021-107
Preprint. Discussion started: 8 November 2021

Down], x is positive in the nominal vehicle direction of motion (forward), y is to the right (starboard) and z is positive in the down direction.

3 Processing

Before converting the raw data from the shear probes into physical units, the MR timestamp was corrected against the AUV data. When the shear probe travels through the water horizontally along axis x, at speed U, then the voltage E_p produced by the probe in response to a cross axis velocity v is given by

$$E_p = 2\sqrt{2}\hat{s}Uv \ , \tag{2}$$

where the constant $\hat{s}$ is the sensitivity of the probe which must be determined by calibration (Lueck et al., 2002). The probe voltage is then converted to shear, $\partial v/\partial x$, in physical units as

$$\frac{\partial v}{\partial x} = \frac{1}{U}\frac{\partial v}{\partial t} = \frac{1}{2\sqrt{2}\hat{s}U^2}\frac{dE_p}{dt} \ , \tag{3}$$

by using the known sensitivity of the shear probe and the travel speed of the AUV (Lueck et al., 2002). The time derivative of E_p is obtained from the differentiator in the electronics of the shear probe, with a known gain. A second probe oriented orthogonal to the first one similarly measures $\partial w/\partial x$. An initial high pass filtering at 0.6 Hz of the shear and vibration signals was performed in order to exclude signals at scales larger than the AUV (about 2 meters). In addition, both shear and vibration signals were despiked before calculating shear spectrum.

Shear spectra are used to estimate the dissipation rate of turbulent kinetic energy, ε. The dissipation rate is proportional to the variance of shear contained at scales from $\mathcal{O}(1)$ m to $\mathcal{O}(10^{-2})$ m. The time series from each shear probe was segmented into half overlapping 8-s long portions, corresponding to roughly 10 m portions along the transects. A fast Fourier transformation (FFT) length corresponding to 1 s was chosen, and each 1-s segment was detrended, and smoothed using a Hanning window, before calculating the shear frequency spectrum for each 8-s segment.

Shear spectra were converted from frequency, f, domain to wavenumber, k, domain using Taylor's frozen turbulence hypothesis and the AUV speed, U, as $k = f/U$. A Doppler Velocity Log (DVL) on the AUV measured U, and the average value for each 8-s segment was used in the conversion. Typical U was 1.1 m s^{-1}, thus the FFT length is equivalent to 1.1 m along-path length, and resolves the low wavenumber part of the spectrum while excluding scales greater than or equal to the vehicle length. For additional cleaning of the shear data, the shear probe signal coherent with the accelerometer data was removed using the method described by Goodman et al. (2006).

Assuming isotropic turbulence, ε was calculated for each segment by integrating the cleaned wavenumber spectrum, $\Psi(k)$ as

$$\epsilon = \frac{15}{2}\nu\overline{\left(\frac{\partial v}{\partial x}\right)^2} = \frac{15}{2}\nu\int_{k_1}^{k_u}\Psi(k)dk \tag{4}$$

https://doi.org/10.5194/os-2021-107
Preprint. Discussion started: 8 November 2021

where ν is the kinematic viscosity and overbar denotes averaging in time (e.g., Fer et al., 2014). The lower (k_1) integration limit is determined by the wavenumber corresponding to the FFT length, and the upper (k_u) integration limit is determined from a minimum in a low-order polynomial fit to the wavenumber spectrum in log-log space. Typically electronic noise takes over after the minimum in the spectrum. To account for the variance in the unresolved (excluded) part of the spectrum, the empirical model for turbulence spectrum determined by Nasmyth (1970) was used. When using two shear probes, the dissipation rate in the segment is calculated as the average of the values from both sensors as long as they agree within a factor of 5, otherwise the minimum of the two was used.

From dissipation estimate time series, we extracted sections when the AUV performed horizontal transects at approximately constant depth with the propeller set to 1500 rotations per minute (RPM). During the horizontal transects the angle of attack (AOA), the difference between the pitch and the direction of travel, was much smaller ($< 3°$) than the critical value of $\pm 20°$ for when the flow over the shear probe is no longer laminar (Osborn and Crawford, 1980). Final data screening excluded data with rate of change exceeding 10, 5 and 2 units per 1 s for roll, pitch and RPM, respectively.

4 Results

Five transects at depths 10, 20, 30, 40, and 50 m were planned across the temperature front, however, the mission ended abruptly after three transects due to a leak in the main hull of the AUV. Data recovered from the three transects are sufficient for the purpose for this technical note. Flight kinematics measured by the AUV are shown in Figure 3. Pitch was in general less than 2.5° and roll was less than 7.5°. The relatively large average roll is probably a result of positioning of the MR relative to the AUV, and the peak roll early in transect two is when the AUV made an abrupt turn (see figure 1b). Note that when the rate of change of roll, pitch and RPM was large, the dissipation rate data was excluded (Sect. 3). The propeller rate was set constant at 1500 RPM, yet the speed past the instrument varied between 1 and 1.2 m s^{-1}, seemingly related to the transition between the water masses (Figures 3b and c).

An RPM of 1500 corresponds to 25 Hz, or using a mean speed of 1.1 m s^{-1} to 23 cycles per meter (cpm). Figure 4a and b show shear spectra in frequency space using 8-s long records (length used for single dissipation estimates), for a moderate and a high value of ε, respectively. Corresponding vibration spectra from the accelerometers are also shown. The contamination of the shear spectra by the propeller at 25 Hz is clearly visible, and the harmonics of the propeller frequency stand out as significant peaks at integer multiples of 25 Hz. In addition, the accelerometers indicate that vibrations between 15 and 20 Hz also affect the shear signal; however, the source of these vibrations is not identified. The cleaned frequency spectra (bold lines) show that contamination from instrument vibration has been successfully removed, and that the spectra resemble the empirical Nasmyth spectra (background gray dashed lines) (Nasmyth, 1970). The shear spectra in wavenumber domain, for the same values of ε as in (a) and (b), are shown in Figure 4c and d. In general, shear probe 1, $\partial w/\partial x$, is able to resolve somewhat higher wavenumbers than shear probe 2, $\partial v/\partial x$. For moderate ε, shear probes 1 and 2 resolve wavenumbers up to 40 and 30 cpm respectively, while for high ε they resolve wavenumbers up to 85 and 65 cpm, respectively. Beyond the resolved part

https://doi.org/10.5194/os-2021-107
Preprint. Discussion started: 8 November 2021

Ocean Science
Discussions
Open Access
EGU

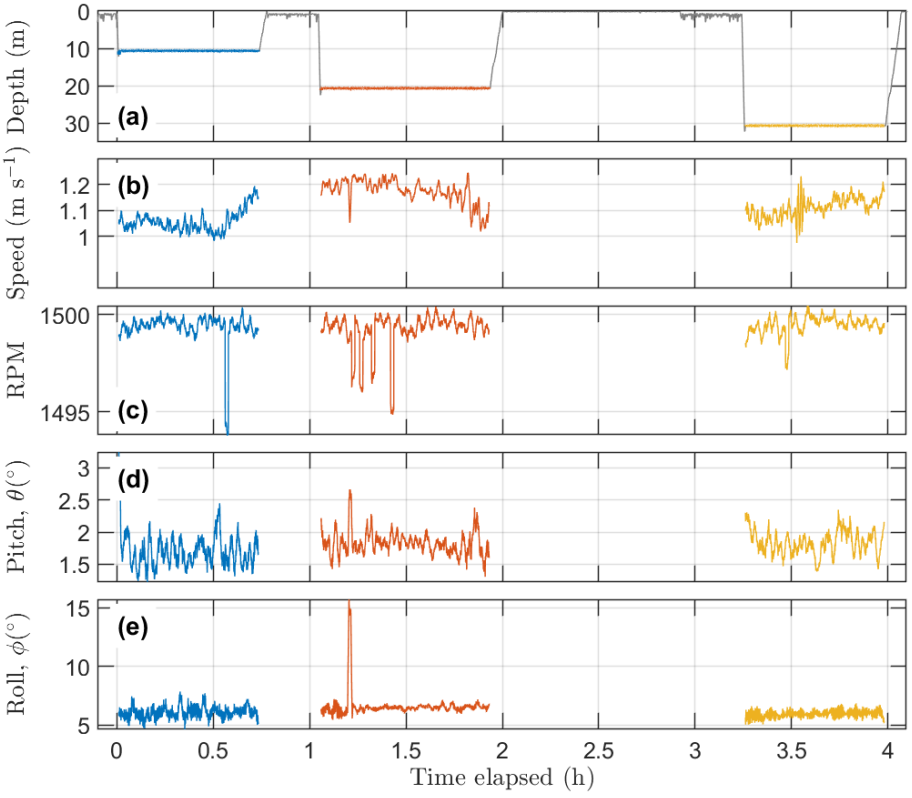

Figure 3. Flight kinematics from AUV. Time series of **a)** depth, **b)** speed past the instrument, **c)** rotation per minute (RPM), **d)** pitch and **e)** roll. Time elapsed is from 26 February 0806 UTC. Selected transects at approximately 10, 20 and 30 m are shown.

of the spectrum, noise levels become too large, and the shear spectrum deviates significantly from the empirical Nasmyth spectrum.

While Figure 4 shows single spectrum for moderate and high values of ε, spectra averaged in bins of ε are useful to document the general data quality at different ε ranges. Figure 5a and b show bin-averaged clean spectra in wavenumber domain (color coded) for $\partial w/\partial x$ and $\partial v/\partial x$, respectively (values limiting the bins are listed in the caption).

For $\varepsilon > 10^{-7}$ W kg^{-1} (purple, yellow and red lines) the spectra closely resemble the bin-averaged Nasmyth spectra (solid gray lines). However, the roll off in the dissipation subrange starts earlier than that indicated in the Nasmyth spectra, suggesting the most energetic dissipation rates are not fully resolved. This is discussed more in Section 5. Comparing $\partial w/\partial x$ to $\partial v/\partial x$, we observe that $\partial w/\partial x$ is generally capable of resolving wavenumbers 10-20 cpm higher than $\partial v/\partial x$. For $\varepsilon < 10^{-7}$ W kg^{-1} (green and blue lines) the bin-averaged spectra start deviating from the empirical Nasmyth spectra significantly for wavenumbers below 4 cpm, especially for $\partial v/\partial x$. While the difference in data quality delivered by the two probes is less than ideal, it is expected that the shear probes oriented orthogonally will sense the vehicle motion differently. Vehicle motion and noise sources are discussed further in Section 5.

https://doi.org/10.5194/os-2021-107
Preprint. Discussion started: 8 November 2021

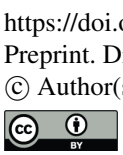

Ocean Science
Discussions
Open Access
EGU

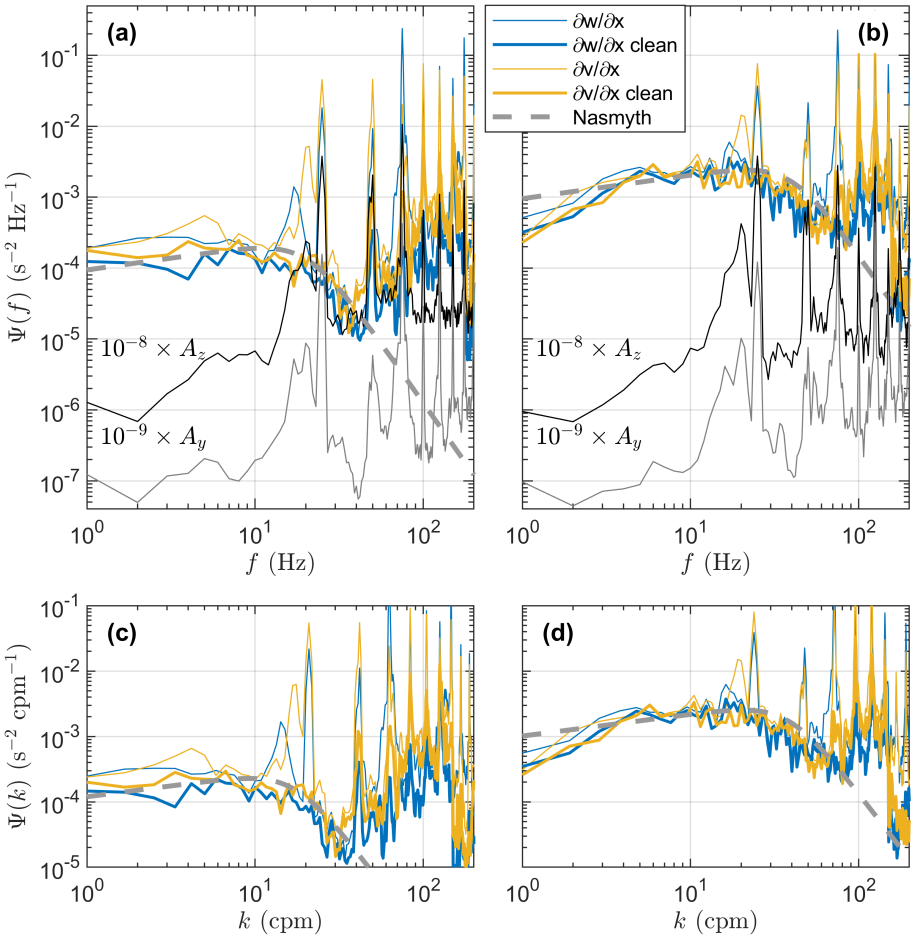

Figure 4. Example frequency spectra with **a)** moderate ($\varepsilon = 5.7 \times 10^{-8}\,\mathrm{W\,kg^{-1}}$), and **b)** high ($\varepsilon = 1.4 \times 10^{-6}\,\mathrm{W\,kg^{-1}}$) dissipation rates, using 8-s long records. Vibration spectra along the instrument's main and transverse axes are also shown with an offset as indicated. Cleaned spectra as indicated by the legend show frequency spectra after removing the shear probe signal coherent with accelerometer signal. Empirical Nasmyth spectra are shown for the values of ε. **c** and **d** show the same shear spectra as (a) and (b) respectively, but in the wavenumber domain. $\partial w/\partial x$ and $\partial v/\partial x$ are shear probes 1 and 2, respectively, on the MicroRider.

https://doi.org/10.5194/os-2021-107
Preprint. Discussion started: 8 November 2021

Ocean Science
Discussions
Open Access
EGU

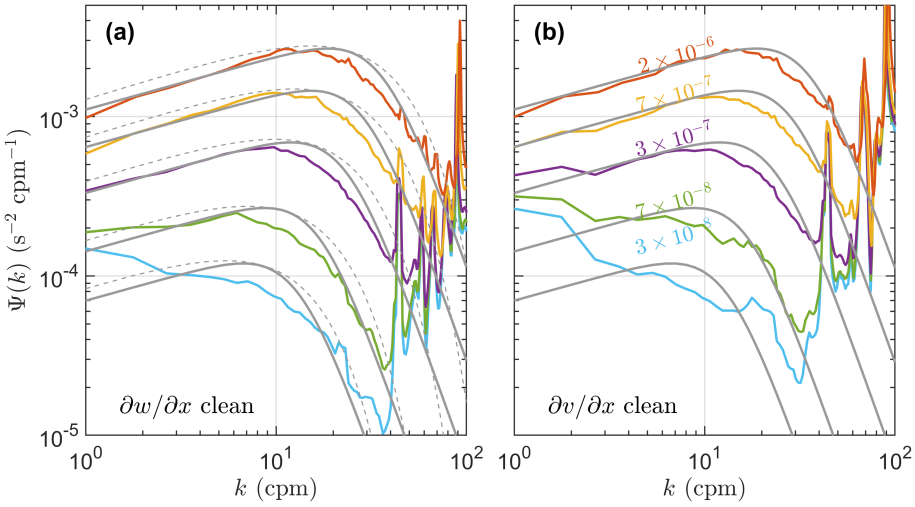

Figure 5. Wavenumber shear spectra of **a)** cleaned $\partial w/\partial x$ (shear probe 1), and **b)** cleaned $\partial v/\partial x$ (shear probe 2) averaged in increasing bins of dissipation rate estimates using data from all depths. Bin averaging limits are set to 1×10^{-8}, 5×10^{-8}, 1×10^{-7}, 5×10^{-7}, 1×10^{-6} and 5×10^{-6}, averaging over 210, 145, 827, 466 and 382 ($\partial w/\partial x$) and 186, 146, 748, 529, 415 ($\partial v/\partial x$) spectra. Bin-averaged values of ε with units in W kg^{-1} are only shown in (b) as they were very similar for both probes. Solid gray background curves are the bin-averaged Nasmyth spectra over all individual Nasmyth spectra in the dissipation bins. Dashed gray lines in (a) show the theoretical Panchev-Kesich spectra for the bin-averaged values of ε.

As ε is calculated from the individual shear wavenumber spectra (Eq. 4), we expect some differences in ε calculated from $\partial w/\partial x$ (ε_1) and ε calculated from $\partial v/\partial x$ (ε_2). Figure 6 compares ε_1 and ε_2 calculated from the two different probes. The scatter plot shows that the two probes agree well within a factor of two for $\varepsilon > 5\times10^{-8}$ W kg^{-1}, below which ε_2 overestimates by a factor of two (Figure 6a). The probability distribution function (PDF) for ε_1 and ε_2 (Figure 6b) show that the two probes in general agree very well for $\varepsilon > 10^{-7}$ W kg^{-1}. For comparison of the three transects conducted by the AUV, we show PDFs of ε_1 and ε_2 at 11, 21, and 31 m depth (Figure 6c, d and e, respectively). While the PDFs at 11 and 21 m depth resemble log-normal or skewed log-normal distributions where ε_1 and ε_2 typically agree (Fig. 6c, d), the PDF at 31 m depth differs. At this deeper transect, a larger portion of the ε measurements is below 10^{-7} W kg^{-1}. The distribution is not log-normal. A second mode appears in low dissipation rates, particularly for ε_2, suggesting noise contributes significantly to the measurements at 31 m depth.

For additional quality control, we compare the final estimate of ε to dissipation measurements from a vertical microstructure profiler collected near the AUV transects (see Figure 1b) at the same time as the AUV transects were conducted. The temperature sampled along the three transects at 11, 21, and 31 m depth, and the corresponding dissipation rates are shown in Figure 7a and b respectively. The dissipation rate of TKE varies throughout the different transects, but generally becomes smaller at greater depth, which is expected in the boundary layer. The maximum likelihood estimate of the horizontal transects (including 95 % confidence intervals) are compared to vertical microstructure profiles sampled by an MSS-90 from Sea and

https://doi.org/10.5194/os-2021-107
Preprint. Discussion started: 8 November 2021

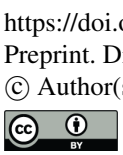

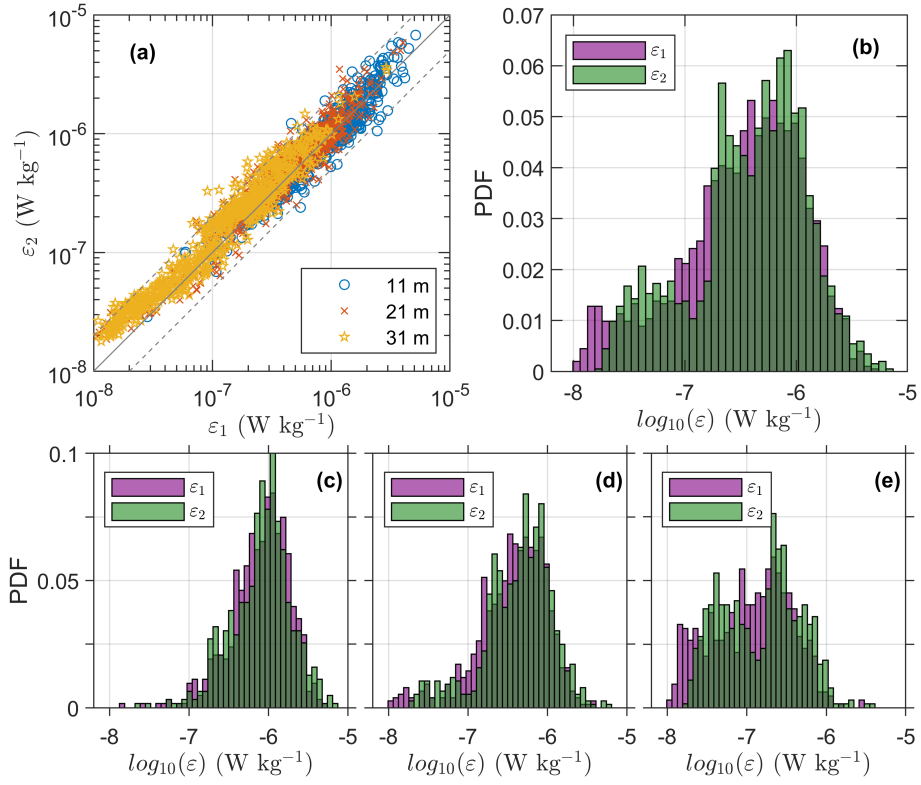

Figure 6. Comparison of dissipation estimates from two probes. ϵ_1 is from $\partial w/\partial x$ measurements, and ϵ_2 is from $\partial v/\partial x$. **a)** Scatter plot of dissipation estimates from each probe, color coded with respect to measurement depth. Gray dashed lines span the agreement within a factor of 2. **b)** Probability distribution function (PDF) for dissipation rates from each probe, using data from all depths. **c)**, **d)**, **e)** PDFs for dissipation rates from each probe, using data from 11, 21 and 31 m depth, respectively.

Sun Technology (Figure 7c). Although the spatial variability of ε is known to be large (Yamazaki et al., 1990), the vertical profiles and the horizontal transects agree within uncertainties.

5 Discussion

While microstructure measurements from gliders and larger AUVs have been extensively tested, microstructure measurements from smaller AUVs have not. Although the Light AUV is both more affordable and easier to handle than its larger siblings, it potentially comes with drawbacks. Being lighter could make the AUV more susceptible to body motion and vibration, potentially contaminating the microstructure measurements. In addition, when the AUV platform is only a few times larger than the MR, AUV maneuvering skills suffer from the added drag from the MR.

Vehicle vibrations contaminate the shear spectra in the 10–30 Hz band (9–27 cpm), where the narrow-band peak at 25 Hz (and its higher harmonics) comes from the propeller (Figure 4). Particularly, the vibrations detected between 10 and 20 Hz

https://doi.org/10.5194/os-2021-107
Preprint. Discussion started: 8 November 2021

Ocean Science
Discussions
Open Access
EGU

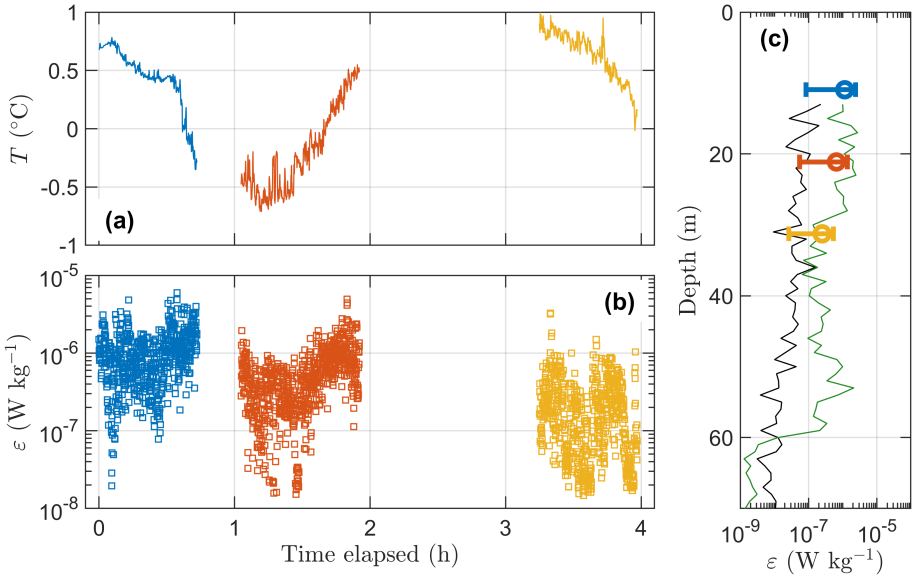

Figure 7. Overview of dissipation rates. Time series of **a)** temperature and **b)** final estimate of the dissipation rate. **c)** Vertical profiles (black and green) of ε measured by the vertical microstructure profiler at two co-located stations marked by stars in Fig. 1b. Maximum likelihood estimator value and the lower and upper limits (95%) for the AUV-MR measurement are shown at their corresponding average depth in (c). Blue, red and yellow corresponds to 11, 21 and 31 m depth respectively.

(9–18 cpm) are worrisome as this is where the roll-off of the turbulence spectrum typically occurs. Nevertheless, removal of the shear probe signal coherent with the accelerometer signal produces clean spectra comparable to the empirical Nasmyth spectrum and the theoretical Panchev-Kesich spectrum. It is only when bin-averaging the shear spectra that we see a potential systematic flaw in the data quality (Figure 5). The results suggest the most energetic wavenumbers are not fully resolved by our instrumentation, i.e. the transition between the inertial subrange and the dissipation subrange drops off short of the bin-average Nasmyth spectra (solid gray lines). Some of the discrepancies between the observed and the Nasmyth spectra are likely caused by the nature of averaging spectra over variable dissipation values, where the maximum in spectrum shifts to higher wavenumbers with increasing ε, which will smooth and smear off the spectral roll-off. To mimic the effect of smoothing of the spectral roll-off, we bin-average individual Nasmyth spectra similarly. Another possible reason for the difference between the observed and the Nasmyth spectra is that the removal of the shear probe signal coherent with the accelerometer signal likely removes some real signal, as the real signal would be indistinguishable from the vibrations caused by the AUV (Palmer et al., 2015). This likely leads to a reduction of variance in the contaminated band between 10–20 Hz (9–27 cpm).

The average wavenumber spectra for the smaller dissipation rates (Figure 5, blue and green lines) deviate from the Nasmyth shape for small wavenumbers. Combined with the issues resolving the spectral roll-off, this suggests the instrument is not able to resolve dissipation rates smaller than about $5 \times 10^{-8}\,\mathrm{W\,kg^{-1}}$. This is particularly problematic for $\partial v/\partial x$ (ε_2). For $\varepsilon < 5 \times 10^{-8}\,\mathrm{W\,kg^{-1}}$, there is a systematic offset between the two shear probes in low wavenumber part of the spectrum (<

https://doi.org/10.5194/os-2021-107
Preprint. Discussion started: 8 November 2021

3 cpm), and ε_2 estimates are relatively strongly affected by the platform motion (Figure 6a). This difference is likely a result of how the two probes react differently to changes in pitch, roll and yaw. While $\partial v/\partial x$ will be affected by roll and by yaw fluctuations, $\partial w/\partial x$ will be affected by changes in pitch but should be fairly insensitive to changes in roll and yaw. However, the effect of pitch, yaw and roll on the shear sensors is also dependent of how the MR is mounted on the AUV.

When mounting the MR on the AUV, our main concern was to ensure that the shear sensors protruded outside the region of flow deformation, without modifying the AUV itself. To avoid interfering with the acoustic modem and fluorescence sensor on the upper part of the AUV, our solution was to make brackets and mount the MR below the AUV. This solution led to unwanted pitching at higher velocities due to the change in center of drag. An alternative solution would be to re-design the wet-section (nose) of the AUV to fit the MR. This could reduce the vehicle vibrations sensed by the MR, and would likely lead to better AUV maneuverability and potentially reduce pitch, roll and yaw.

6 Summary and Conclusions

A modified MicroRider-1000LP was mounted below a Light AUV and deployed in the Barents Sea during a cruise in February 2021. The AUV conducted three transects across a surface temperature front at 11, 21 and 31 m depth, while continuously sampling microstructure shear. Dissipation rate of turbulent kinetic energy is estimated from the shear measurements. Although the vibrations of the AUV contaminate the shear probe records, the shear spectra for dissipation levels above 5×10^{-8} W kg^{-1} are sufficiently cleaned using the Goodman method (Goodman et al., 2006). Dissipation rates measured from the AUV agree well with the measurements using a loosely-tethered vertical microstructure profiler from the ship. The overall noise level from the AUV is quite large, however. This setup cannot detect dissipation rates below 5×10^{-8} W kg^{-1} reliably, and is unfit for use in quiescent boundary layers. An improved installation of the turbulence probes on the nose of the AUV could reduce some of the limitations reported here and allow acceptable quality dissipation measurements from the AUV in relatively quiet environments.

Data availability. The AUV and MicroRider data set is available from Fer et al. (2021) through the Norwegian Marine Data Centre, https://doi.org/10.21335/NMDC-1821443450 with a Creative Commons Attribution 4.0 International License. SST data are obtained from the EU Copernicus Marine Service Information, product SEAICE_ARC_SEAICE_L4_NRT_OBSERVATIONS_011_008.

Author contributions. IF, TM-B and EHK collected the data, conceived and planned the analysis. IF and EHK performed the analysis. EHK wrote the paper, with advice and critical feedback from IF and TM-B. All authors discussed the results and finalized the paper.

Competing interests. Authors have no competing interests. IF is a member of the editorial board for the Ocean Science

https://doi.org/10.5194/os-2021-107
Preprint. Discussion started: 8 November 2021

Acknowledgements. The research was funded by the Research Council of Norway through the Nansen Legacy project (276730). We thank the officers and crew of the Kronprins Haakon for their skillful operations, the cruise leader Frank Nilsen for supporting the experiment. Martin Ludvigsen facilitated the AUV and provided valuable advise in preparations and planning. We thank Rolf Lueck and Evan Cervelli at Rockland Scientific for their advice and assistance in modifying the MicroRider for the AUV application. The Nansen Legacy uses NIRD as data depository (account numbers NS9610K and NS9530K). Figure 1a is produced using E.U. Copernicus Marine Service Information.

https://doi.org/10.5194/os-2021-107
Preprint. Discussion started: 8 November 2021

References

Dhanak, M. R. and Holappa, K.: An Autonomous Ocean Turbulence Measurement Platform, Journal of Atmospheric and Oceanic Technology, 16, 1506–1518, https://doi.org/10.1175/1520-0426(1999)016<1506:AAOTMP>2.0.CO;2, publisher: American Meteorological Society Section: Journal of Atmospheric and Oceanic Technology, 1999.

Fer, I., Peterson, A. K., and Ullgren, J. E.: Microstructure Measurements from an Underwater Glider in the Turbulent Faroe Bank Channel Overflow, Journal of Atmospheric and Oceanic Technology, 31, 1128–1150, https://doi.org/10.1175/JTECH-D-13-00221.1, 2014.

Fer, I., Mo-Bjørkelund, T., and Kolås, E. H.: Dissipation measurements from AUV transects across a surface temperature front in the Barents Sea, https://doi.org/https://doi.org/10.21335/NMDC-1821443450, 2021.

Frajka-Williams, E., Brearley, J. A., Nash, J. D., and Whalen, C. B.: Chapter 14 - New technological frontiers in ocean mixing, in: Ocean Mixing, edited by Meredith, M. and Garabato, A. N., pp. 345–361, Elsevier, https://doi.org/10.1016/B978-0-12-821512-8.00021-9, 2022.

Garabato, A. C. N., Frajka-Williams, E. E., Spingys, C. P., Legg, S., Polzin, K. L., Forryan, A., Abrahamsen, E. P., Buckingham, C. E., Griffies, S. M., McPhail, S. D., Nicholls, K. W., Thomas, L. N., and Meredith, M. P.: Rapid mixing and exchange of deep-ocean waters in an abyssal boundary current, Proceedings of the National Academy of Sciences, 116, 13 233–13 238, https://doi.org/10.1073/pnas.1904087116, 2019.

Goodman, L., Levine, E. R., and Lueck, R. G.: On Measuring the Terms of the Turbulent Kinetic Energy Budget from an AUV, Journal of Atmospheric and Oceanic Technology, 23, 977–990, https://doi.org/10.1175/JTECH1889.1, 2006.

Gregg, M. C.: Ocean Mixing, Cambridge University Press, https://doi.org/10.1017/9781316795439, 2021.

Jakobsson, M., Mayer, L., Coakley, B., Dowdeswell, J. A., Forbes, S., Fridman, B., Hodnesdal, H., Noormets, R., Pedersen, R., Rebesco, M., Schenke, H. W., Zarayskaya, Y., Accettella, D., Armstrong, A., Anderson, R. M., Bienhoff, P., Camerlenghi, A., Church, I., Edwards, M., Gardner, J. V., Hall, J. K., Hell, B., Hestvik, O., Kristoffersen, Y., Marcussen, C., Mohammad, R., Mosher, D., Nghiem, S. V., Pedrosa, M. T., Travaglini, P. G., and Weatherall, P.: The International Bathymetric Chart of the Arctic Ocean (IBCAO) Version 3.0, Geophysical Research Letters, 39, n/a–n/a, https://doi.org/10.1029/2012gl052219, 2012.

Levine, E. R. and Lueck, R. G.: Turbulence Measurement from an Autonomous Underwater Vehicle, Journal of Atmospheric and Oceanic Technology, 16, 1533–1544, https://doi.org/10.1175/1520-0426(1999)016<1533:TMFAAU>2.0.CO;2, publisher: American Meteorological Society Section: Journal of Atmospheric and Oceanic Technology, 1999.

Lueck, R. G.: Horizontal and vertical turbulence profilers, in: Marine Turbulence: Theories, observations and models. Results of the CARTUM project., edited by Baumert, H. Z., Simpson, J. H., and Sündermann, J., pp. 89–100, Cambridge University Press, Cambridge, UK, 2005.

Lueck, R. G., Wolk, F., and Yamazaki, H.: Oceanic Velocity Microstructure Measurements in the 20th Century, Journal of Oceanography, 58, 153–174, https://doi.org/10.1023/A:1015837020019, 2002.

McPhail, S., Templeton, R., Pebody, M., Roper, D., and Morrison, R.: Autosub Long Range AUV Missions Under the Filchner and Ronne Ice Shelves in the Weddell Sea, Antarctica - an Engineering Perspective, in: OCEANS 2019 - Marseille, pp. 1–8, https://doi.org/10.1109/OCEANSE.2019.8867206, 2019.

Nasmyth, P. W.: Oceanic turbulence, Ph.D. thesis, University of British Columbia, https://doi.org/10.14288/1.0302459, 1970.

Nilsen, F., Fer, I., Baumann, T. M., Breivik, Ø., Czyz, C., Frank, L., Kalhagen, K., Koenig, Z., Kolås, E. H., Kral, S. T., Mabrouk, B. M. A., Mo-Bjørkelund, T., Muller, M., and Rabault, J.: Nansen Legacy Cruise PC-2: Winter Process Cruise. Nansen Legacy Report Series, 2021.

https://doi.org/10.5194/os-2021-107
Preprint. Discussion started: 8 November 2021

Osborn, T. R. and Crawford, W. R.: An airfoil probe for measuring turbulent velocity fluctuations in water, in: Air–Sea Interaction: Instruments and Methods, edited by Dobson, F., Hasse, L., and Davis, R., pp. 369–386, Plenum Press, New York, 1980.

OSI SAF: Global Sea Ice Concentration (netCDF) - DMSP, https://doi.org/10.15770/EUM_SAF_OSI_NRT_2004, 2017.

Palmer, M., Stephenson, G., Inall, M., Balfour, C., Düsterhus, A., and Green, J.: Turbulence and mixing by internal waves in the Celtic Sea determined from ocean glider microstructure measurements, Journal of Marine Systems, 144, 57–69, https://doi.org/10.1016/j.jmarsys.2014.11.005, 2015.

Scheifele, B., Waterman, S., Merckelbach, L., and Carpenter, J. R.: Measuring the Dissipation Rate of Turbulent Kinetic Energy in Strongly Stratified, Low-Energy Environments: A Case Study From the Arctic Ocean, Journal of Geophysical Research: Oceans, 123, 5459–5480, https://doi.org/10.1029/2017JC013731, 2018.

Schultze, L. K. P., Merckelbach, L. M., and Carpenter, J. R.: Turbulence and Mixing in a Shallow Shelf Sea From Underwater Gliders, Journal of Geophysical Research: Oceans, 122, 9092–9109, https://doi.org/10.1002/2017JC012872, 2017.

Sousa, A., Madureira, L., Coelho, J., Pinto, J., Pereira, J., Borges Sousa, J., and Dias, P.: LAUV: The Man-Portable Autonomous Underwater Vehicle, IFAC Proceedings Volumes, 45, 268–274, https://doi.org/10.3182/20120410-3-PT-4028.00045, 2012.

Spingys, C. P., Garabato, A. C. N., Legg, S., Polzin, K. L., Abrahamsen, E. P., Buckingham, C. E., Forryan, A., and Frajka-Williams, E. E.: Mixing and Transformation in a Deep Western Boundary Current: A Case Study, Journal of Physical Oceanography, 51, 1205–1222, https://doi.org/10.1175/JPO-D-20-0132.1, 2021.

Thorpe, S. A., Osborn, T. R., Jackson, J. F. E., Hall, A. J., and Lueck, R. G.: Measurements of Turbulence in the Upper-Ocean Mixing Layer Using Autosub, Journal of Physical Oceanography, 33, 122–145, https://doi.org/10.1175/1520-0485(2003)033<0122:MOTITU>2.0.CO;2, 2003.

Yamazaki, H., Lueck, R. G., and Osborn, T.: A Comparison of Turbulence Data from a Submarine and a Vertical Profiler, Journal of Physical Oceanography, 20, 1778–1786, https://doi.org/10.1175/1520-0485(1990)020<1778:ACOTDF>2.0.CO;2, publisher: American Meteorological Society Section: Journal of Physical Oceanography, 1990.